Journal of Materials Chemistry A

Accepted Manuscript

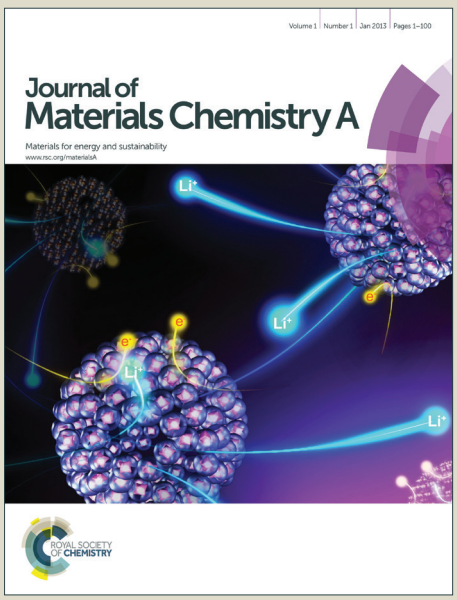

ROYAL SOCIETY OF CHEMISTRY

www.rsc.org/materialsA

Journal Name

ARTICLE

A Graphene-directed Assembly Route to Hierarchically Porous Co-N_x/C Catalysts for High-performance Oxygen Reduction

Received 00th January 20xx,
Accepted 00th January 20xx

DOI: 10.1039/x0xx00000x

www.rsc.org/

Jing Wei[a], Yaoxin Hu[a], Zhangxiong Wu[b], Yan Liang[a], Sookwan Leong[a], Biao Kong[a], Xinyi Zhang[c], Dongyuan Zhao[a,d], George P. Simon[e], Huanting Wang[a]*

The development of non-precious metal catalysts for efficient oxygen reduction is of significance for many advanced electrochemical devices such as fuel cells and metal-air batteries. Herein, we develop a graphene-directed assembly route to synthesize hierarchically nanoporous Co-N_x/C materials with a macro/meso/microporous structure, high specific surface area (i.e. 512 m^2/g) and excellent conductivity using graphene oxide (GO) supported zeolitic imidazolate frameworks nanocrystal arrays as a catalyst precursor, followed by carbonization and acid leaching process. In this route, GO acts as a structure-directing agent to construct ZIF nanocrystal arrays supported on GO nanosheets. During the carbonization process, the resulting reduced graphene oxide functions as a binder and electrical conductor to connect individual ZIF-derived carbon nanoparticles into the macroporous structure and increase the overal conductivity. ZIF nanocrystals themselves are also converted into meso/microporous carbon nanoparticles without using any other template. The hierarchically porous Co-N_x/C materials exhibit high ORR catalytic activity, superior stability and good methanol tolerance in both alkaline and acidic conditions.

Introduction

Oxygen reduction reaction (ORR) is one of the most fundamentally and technologically important reactions in many advanced electrochemical devices such as fuel cells and metal-air batteries.[1-4] Due to sluggish kinetics process of ORR, Pt-based materials have been regarded as the most effective catalysts, and exhibit a relatively low overpotential and high current density.[5] However, they have some drawbacks such as high cost, limited resources, low CO and methanol tolerance and poor durability, which severely hinder the commercialization of these electrochemical devices. To reduce the cost and enhance the durability, Pt-based alloys, low-cost alternatives such as carbon-supported transition-metal/nitrogen (M-N_x/C, M = Fe, Co), perovskites, spinel oxides and metal-free heteroatom-doped carbon nanomaterials have been investigated recently.[6-18] Among them, carbon-supported M-N_x has received considerable attention because of their potential as electrocatalysts with high catalytic activity and selectivity, and excellent durability.[19-26]

A great deal of research has been conducted to synthesize hierarchically nanoporous M-N_x/C (M = Fe, Co) materials with a macro/meso/microporous structure as ORR electrocatalysts.[27-28] Introducing hierarchical nanopores into bulk carbon materials can not only increase their porosity to expose more active sites and enhance mass transport, but also retain high electrical conductivity. It is well accepted that high density of active sites, highly porous structure for fast mass transport and excellent electrical conductivity for fast electron transfer are three key required characteristics for a high-performance electrocatalyst. The hierarchically nanoporous M-N_x/C materials are generally prepared using the external templates such as ordered mesoporous silica, silica colloid, and mixed templates (i.e. Pluronic F127 and polystyrene nanospheres), which suffers some drawbacks such as time-consuming and costly.[26-34] It's still highly desirable to develop a simple template-free method to synthesize hierarchically nanoporous M-N_x/Carbon-based catalysts with high specific surface area and excellent conductivity for significant improvement of their ORR performance for practical applications.

As an important kind of metal organic frameworks, zeolitic imidazolate frameworks (ZIFs) have been considered as attractive catalyst precursors since they contain transition metal ions (Zn^{2+}, Co^{2+}) and N-rich imidazole ligands.[35-45] For instance, ZIF-67 consists of Co^{2+} and imidazole ligand, and contains abundant Co-N_4 coordinate moieties in its framework; in addition, the easy preparation, controllable crystal size, and high specific surface area make ZIF-67 an ideal precursor for the synthesis of Co-N_x/C catalyst with abundant active sites via

[a] Department of Chemical Engineering, Monash University, Clayton, Victoria 3800, Australia. E-mail: huanting.wang@monash.edu
[b] College of Chemistry, Chemical Engineering and Material Science, Soochow University, Suzhou City, Jiangsu, 215123, PR China.
[c] School of Chemistry, Faculty of Science, Monash University, Clayton, Victoria 3800, Australia
[d] Department of Chemistry, Fudan University, Shanghai, P. R. China.
[e] Department of Materials Engineering, Monash University, Clayton, Victoria 3800, Australia.
Electronic Supplementary Information (ESI) available: [details of any supplementary information available should be included here]. See DOI: 10.1039/x0xx00000x

direct carbonization.[39-40] However, most of the ZIF-derived carbon nanoparticles are dispersible, and they cannot form a continuous framework, resulting in the low electronic conductivity which is undesirable for ORR.[41] Graphene with a unique two-dimensional structure and excellent electrical conductivity has been widely studied as a highly promising carbon support for electrocatalysts.[46-49] For instance, Zhong et al recently developed 2D sandwich-like ZIF-8 derived graphene-based nitrogen-doped porous carbon sheets, which showed high ORR performance in alkaline conditions.[41] Hou et al prepared nitrogen-doped graphene/cobalt embedded porous carbon polyhedron through simple pyrolysis of the mixture of graphene oxide and ZIF-67 nanoparticles, which revealed higher electrocatalytic activities than sole ZIF-67 derived carbon for oxygen reduction reaction in alkaline media.[43] In these cases, graphene was used to increase the conductivity of the electrocatalysts and create additional active sites for ORR in alkaline condition by forming N doped graphene. To date, however, there has been few reports focusing on the role of the graphene as a structure-directing agent in the formation of hierarchically 3D porous Co-N_x/C materials via direct carbonization of ZIF materials; such porous electrocatalysts are highly desirable for ORR due to enhance the mass transport and electron transfer. In addition, the ORR performance of ZIF-derived graphene-based catalysts has been mainly investigated in alkaline conditions. Their performance in harsher acidic conditions such as proton exchange membrane fuel cells is yet to be investigated.

Herein, we report a graphene-directed assembly route to synthesize hierarchically nanoporous Co-N_x/C materials with a macro/meso/microporous structure and high specific surface area (i.e. 512 m^2/g) via a simple carbonization of graphene oxide (GO) supported ZIF nanocrystal arrays, followed by acid leaching to remove large Co nanoparticles. In this approach, graphene oxide is employed as a structure-directing agent to prepare ZIF/GO composites. During the carbonization, the resultant reduced graphene oxide acts as a binder and electrical conductor to connect the individual carbon nanoparticles derived from ZIF, forming a macroporous structure with high conductivity. At the same time, ZIF nanocrystals are converted to meso/microporous carbon nanoparticles after carbonization and acid leaching process without involving any other template. The hierarchically nanoporous Co-N_x/C materials are further used as electrocatalysts for ORR, and they show high catalytic activity, superior stability and good methanol tolerance in both alkaline and acidic conditions.

2. Experimental section

2.1 Synthesis of ZIF/rGO-700-AL

Graphene Oxide (GO) was prepared via modified Hummer method.[50] 0.45 g of $Co(NO_3)_2{\cdot}6H_2O$ and 5.5 g of 2-methylimidazole were dissolved in 3 and 20 mL of water respectively. Then, $Co(NO_3)_2$ solution (3 mL) was added into the 2-methylimidazole solution to obtain a purple solution. 3 mL of GO solution (10 mg/mL) was added to the above mixed solution immediately. After 5 h, the precipitation was collected by centrifugation (8000 rpm for 2 min) and washing with water at least three times to remove the dissociative the ZIF crystals and other species. After drying at 80 ^oC for 12 h, ZIF/GO was prepared. ZIF/GO was then calcined at 700 ^oC for 3 h in Ar atmosphere to obtain ZIF/rGO-700. To remove the Co particles, ZIF/rGO-700 was immersed in 6 M HCl solution for 12 h and then collected by centrifugation and washing with water. After drying at 80 ^oC, ZIF/rGO-700-AL was prepared. The synthesis of ZIF-700-AL was similar to ZIF/rGO-700-AL without the addition of GO solution.

2.2 Characterization

Scanning electron microscopy (SEM) images were taken with a field-emission scanning electron microscope (FEI Nova NanoSEM 450) operating at 5 kV. Transmission electron microscopy (TEM) images were taken by a JEOL 2100F FEG TEM (Japan) and FEI Tecnai G2 T20 operated at an accelerating voltage of 200 kV. The samples were first dispersed in ethanol. A drop of the dispersion was supported on a copper grid with holey carbon films and then dried, prior to TEM characterization. Nitrogen adsorption/desorption isotherms were measured at -196 °C with a Micromeritics ASAP 2010 analyzer. Before measurements, the samples were degassed in a vacuum at 180 °C for at least 8 h. The Brunauer-Emmett-Teller (BET) method was utilized to calculate the specific surface area by using the adsorption data at p/p_0 range of 0.05 ~ 0.25. The Raman spectra was measured on WITEC Alpha 300 confocal micro-Raman system equipped with a 532 nm laser source and 100X objective lens. X-ray photoelectron spectroscopy (XPS) experiments were carried out on a Kratos AXIS Ultra DLD system with Al Kα radiation as X-ray source for radiation. Powder X-ray diffraction (PXRD) patterns were recorded in the 2θ range of 5–80° at room temperature using a Miniflex 600 diffractometer (Rigaku, Japan) in transmission geometry using Cu Kα radiation (15 mA and 40 kV) at a scan rate of 2 °/min and a step size of 0.02°.

2.3 Electrochemical measurements

Cyclic voltammetry (CV) and linear sweep voltammetry (LSV) voltammetry were performed by using a μAutolab electrochemical analyzer in a conventional three-electrode electrochemical cell. A Pt wire auxiliary electrode, a saturated Ag/AgCl (saturated with 3 M KCl) reference electrode, and rotating disk working electrode were used. For the oxygen reduction reaction (ORR), 8 mg of catalysts (or 2 mg of commercial Pt/C, 20 wt%, from Sigma-Aldrich) were dispersed in 1 mL of ethanol (containing 0.03 mL of 5.0 wt % Nafion) solution under ultrasonic agitation to form an electrocatalyst ink. Then 10 μL of the electrocatalyst ink was dropped on the surface of the pre-cleaned rotating disk electrode (5 mm diameter, 0.196 cm^2) and dried at room temperature. A 0.1 M KOH (or 0.1 M $HClO_4$) solution was used as the electrolyte for all the CV and RDE studies. Argon and O_2 were used to achieve oxygen-free and oxygen-rich environments. The electrolyte was saturated with Ar (or O_2) before test. The CV curves were recorded at a scan rate of 50 mV/s; the RDE curves were

recorded at a scan rate of 10 mV/s. A flow of O_2 was maintained over the electrolyte during the CV and LSV test to ensure O_2 saturation. The numbers of electrons transferred (n) during ORR was calculated by Koutecky-Levich equation, at various electrode potentials:

$$\frac{1}{J}=\frac{1}{J_L}+\frac{1}{J_K}=\frac{1}{B\omega^{0.5}}+\frac{1}{J_K}$$

$$B=0.62nFC_0D_0^{2/3}v^{-1/6}$$

where J is the measured current density, J_K and J_L are the kinetic and diffusion-limiting current densities, ω is the angular velocity, n is transferred electron number, F is the Faraday constant (96485 C mol^{-1}), C_0 is the bulk concentration of O_2 (1.2×10^{-6} mol cm^{-3} for 0.1 M KOH, 1.26×10^{-6} mol cm^{-3} for 0.1 M $HClO_4$), D_0 is the diffusion coefficient of O_2 (1.9×10^{-5} cm^2 s^{-1} in 0.1 M KOH, 1.93×10^{-5} cm^2 s^{-1} in 0.1 M $HClO_4$), and v is the kinematic viscosity of the electrolyte (0.01 cm^2 s^{-1} in 0.1 M KOH, 0.01009 cm^2 s^{-1} in 0.1 M $HClO_4$).

3. Results and Discussion

The synthesis of hierarchically porous Co-N_x/C materials is schematically illustrated in **Figure 1**. In the first step, GO aqueous solution was added immediately after the formation of ZIF seeds in water at room temperature. Due to the coordination interactions between the metal ion (Co^{2+}) from ZIF cluster and oxygen contained groups (such as epoxy and hydroxyl) from the GO sheet, the crystal seeds can be well attached onto either side of GO layer. After ZIF crystallization at room temperature for 5 h, ZIF nanocrystal arrays supported on GO sheets (denoted as ZIF/GO) could be obtained by washing away loosely attached ZIF nanocrystals with deionized water. In the second step, the ZIF/GO composites were pyrolyzed in Ar at 700 °C for 3 h to get macroporous carbon

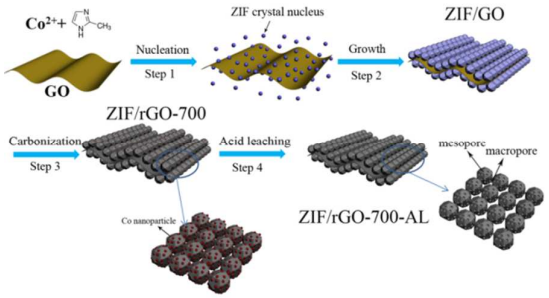

Figure 1. The synthesis procedure of the hierarchically nanoporous Co-N_x/C materials (ZIF/rGO-700-AL). Step 1, the nucleation of ZIF seeds on either side of a graphene oxide (GO) nanosheet. Step 2, the growth of ZIF nanocrystal arrays supported on a GO nanosheet (ZIF/GO). Step 3, carbonization of GO supported ZIF nanocrystal arrays at 700 °C in Ar atmosphere to obtain macroporous Co-N_x/C material (ZIF/rGO-700). Step 4, acid leaching to remove large Co nanoparticles and hence produce meso/microporous structure (ZIF/rGO-700-AL).

composite (denoted as ZIF/rGO-700). During the carbonization process, the catalytically active sites Co-N_x could be formed inside the carbon material. The excessive Co species tended to aggregate to form large Co nanoparticles. At the same time, the GO was converted into reduced GO (rGO) at a high temperature. As strong interactions between ZIF crystals and GO, the rGO could act as a binder to connect the ZIF-derived nanoparticles. In the third step, the fully opened framework with mesoporous and microporous structure was obtained after the removal of Co nanoparticles inside carbon particles through acid leaching. The samples were denoted as ZIF/rGO-700-AL.

Scanning electron microscope (SEM) image of ZIF/GO composite shows a layered structure with a large area (**Figure 2a**), indicating a successful synthesis of ZIF nanocrystal arrays supported on GO nanosheets. A high-resolution SEM image shows that the ZIF nanocrystals aggregate together to form continuous arrays, which are wrapped by a GO layer (**Figure 2b, Figure S1a, b**). After carbonization at 500 °C in Ar, SEM image of ZIF/rGO-500 reveals obviously shrinkage for both ZIF crystals and graphene oxide (Figure S1c, d). The samples calcined at 700 °C (ZIF/rGO-700) show a macroporous structure, which is constructed by secondary assembly of ZIF-derived carbon nanoparticles (Figure 2c). The macroporous structure is obtained by severe shrinkage of ZIF crystals and GO during carbonization process. The reduced graphene oxide (rGO) obtained by high temperature reduction of GO acts as a binder to fix the macroporous structure via connecting the ZIF-

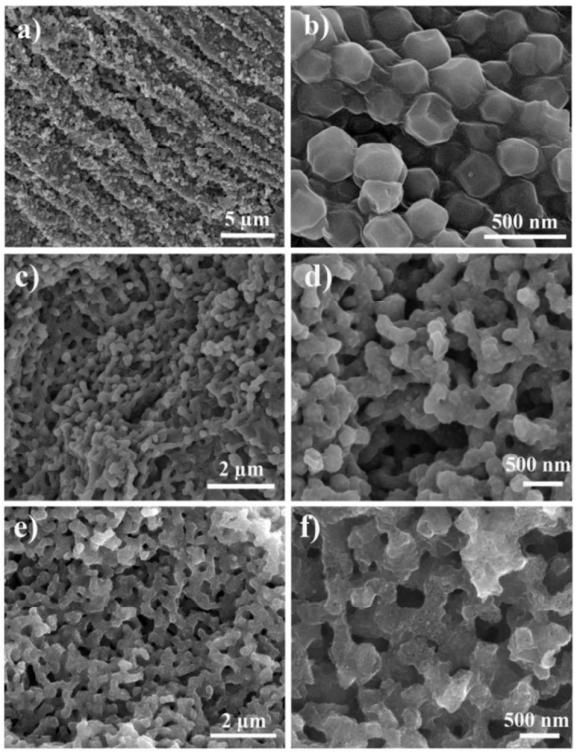

Figure 2 SEM images of a, b) ZIF/GO, c, d) ZIF/rGO-700, e, f) ZIF/rGO-700-AL.

derived carbon nanoparticles. Co nanoparticles are also formed after carbonization, which are embedded in the ZIF-derived carbon particles (Figure 2d). The Co nanoparticles are unstable in acidic ORR medium, so they are subsequently removed via acid leaching (AL) using 6 M HCl aqueous solutions. After acid leaching, SEM image reveals that ZIF/rGO-700-AL remains as a macroporous structure, implying a stable porous structure under acidic conditions (Figure 2e). Additionally, some mesopores are generated after removal of Co nanoparticles (Figure 2f), indicating that Co nanoparticles inside the carbon matrix act as a mesopore template. To investigate the role of GO in the formation of the macroporous structure, ZIF crystals without addition of GO were also treated by carbonization and acid leaching in the same conditions (denoted as ZIF-700-AL). SEM image shows that ZIF-700-AL is composed of loosely packed nanoparticles, confirming that GO acts as a structure directing agent for the formation of macroporous structure (Figure S2). This kind of hierarchically porous structure may show enhanced electrical conductivity owing to its continuous carbon framework and the existence of highly conductive graphene.

Transmission electron microscopy (TEM) images of ZIF/rGO-700 show the carbon nanoparticles/rGO composited structure. The Co nanoparticles were embedded in the carbon matrix, which is consistent with SEM results (**Figure 3**a). Since the rGO is homogenously and completely coated with ZIF-derived carbon particles, the existence of rGO can be only found at some edges of ZIF/rGO-700 samples. High-resolution TEM (HRTEM) image shows a typical lattice fringe of Co nanoparticle, which is wrapped by the graphite layer (**Figure 3b, c**). Scanning transmission electron microscopy (STEM) images of ZIF/rGO-700 clearly reveal the Co nanoparticles

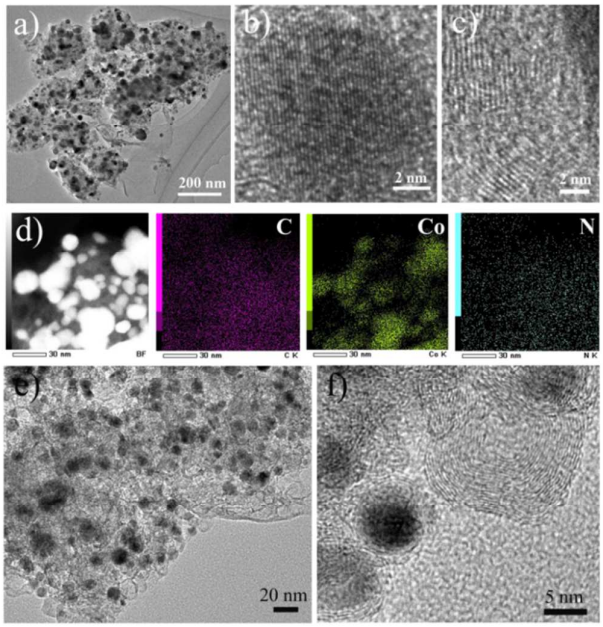

Figure 3 a-c) TEM images, d) STEM image and corresponding element mapping of ZIF/rGO-700; e, f) TEM images of ZIF/rGO-700-AL after acid leaching with 6 M HCl solution.

were embedded in the carbon matrix (**Figure 3d, e**). Elemental mapping results reveal that the N and C elements are uniformly distributed in the carbon framework. Co element signals exist not only in the area of Co nanoparticles (white dots), but also on other areas even without Co nanoparticles observed. These Co species could possibly bond with N atoms to form Co-N active sites. After acid leaching, Co nanoparticles without being fully wrapped by a graphite layer were removed, leaving mesopores in the carbon particles. However, some Co nanoparticles inside the carbon particles are entirely encapsulated by the continuous graphite layer, and they are stable in acid solution and remain in the carbon matrix after acid leaching (**Figure 3e, f**).

The XRD pattern of ZIF/GO shows a typical ZIF-67 phase without impurity (**Figure 4**a). After carbonization, All XRD peaks of the sample arise from Co and CoO phase. The existence of CoO may be due to the oxidation of Co nanoparticles exposed on the surface of carbon particles. After acid leaching, only graphite and Co nanoparticles phase exist. CoO and part of Co nanoparticles accessible to acid can be removed. The half-peak width of Co nanoparticles obviously decreases due to the partial removal of large Co nanoparticles in the carbon particles. The emergence of graphite peak reveals that the content of carbon increases after the removal of Co nanoparticles. Raman spectrum of ZIF/rGO-700-AL displays the D band at 1351 and G band at 1607 cm^{-1}, corresponding to disordered graphitic carbon and the sp^2-bond carbon atoms, respectively (**Figure 4b**). A broad 2D peak further reveals a high degree of graphitization. Elemental analysis results show a high content of N element in ZIF/rGO-700-AL (6.4 wt%), implying that imidazole is a good precursor for the preparation of rich N-doped carbon materials. X-ray photoelectron spectroscopy (XPS) was used to analyse the

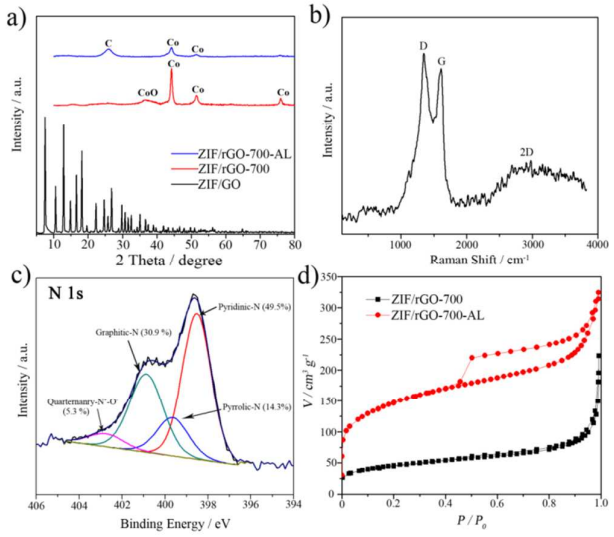

Figure 4 a) XRD patterns, b) Raman spectra, c) high-resolution N 1s spectra, d) N_2 sorption isotherms of ZIF/rGO-700-AL. XRD data of ZIF/GO and ZIF/rGO-700 and N_2 sorption isotherms of ZIF/rGO-700 are also shown in a) and d) respectively.

element-bonding configurations (**Figure 4c**). The high resolution N1s spectra of ZIF/rGO-700-AL can be fitted into four peaks at about 398.5, 399.5, 401.0 and 402.6 eV, corresponding to pyridinic nitrogen, pyrrolic nitrogen, graphitic nitrogen and pyridinic N^+-O^-, respectively. Their relative contents are 49.5, 14.3, 30.9 and 5.4 %, respectively. The N atoms located on the edge of the graphitic sheets such as pyridinic and pyrrolic nitrogen may serve as coordination sites with the metal ions (Co^{2+}), resulting in a high active sites (Co-N_x/C) for ORR. In the Co 2p spectra, the peak at about 780 and 786 eV assigned to Co-N species, while the peaks at 796.5 and 804.6 eV originate from Co-O species (Figure S3).[25] The Co-N and Co-O species can enhance ORR catalytic activity in alkaline conditions, while Co-N sites play a key role in ORR performance in acidic conditions. N_2 sorption isotherms show that the BET surface area and pore volume of ZIF/rGO-700-AL greatly increase from 161 m^2/g and 0.35 cm^3/g to 512 m^2/g and 0.50 cm^3/g respectively after acid leaching of ZIF/rGO-700 (**Figure 4d**). The increase of specific surface area and pore volume is mainly attributed to the removal of dense Co nanoparticles, which also act as templates to generate additional mesopores. The pore size distributions of ZIF/rGO-700-AL show that the sample has both micropores and mesopores (Figure S3). The existence of micropores (1.3 nm) and mesopores (5.3 nm) is beneficial to the catalysts because both the density of active sites and their accessibility by reactants increase.

The ORR activity of ZIF/GO derived catalysts was assessed in both alkaline and acidic conditions using the rotating disk electrode (RDE) technique. The cyclic voltammogram (CV) curves of Pt/C, ZIF/rGO-700, ZIF/rGO-700-AL, and ZIF-700-AL show well-defined cathodic peaks in O_2-saturated 0.1 M KOH compared with that in Ar-saturated solution (Figure S4). The cathodic peaks are at 0.79, 0.81, 0.81 and 0.80 V versus RHE, which implies a high ORR activity for ZIF/GO derived Co-N_x/carbon catalysts. LSV curves show that the onset potentials of Pt/C, ZIF/rGO-700, ZIF/rGO-700-AL, and ZIF-700-AL are 0.90, 0.92, 0.93, and 0.93 V vs. RHE, respectively (**Figure 5**a). All the ZIF/rGO derived carbon materials show a high onset potential. Moreover, the limiting current density of Pt/C, ZIF/rGO-700, ZIF/rGO-700-AL, and ZIF-700-AL at 0.70 V are 4.56, 4.56, 5.49, 4.46 mA cm^{-2}, respectively. As the acid-leaching can remove the dense Co nanoparticles in the carbon matrix and increase the porosity of the carbon framework, which can effectively enhance the transport of reactant and products. In addition, the removal of cobalt nanoparticles may be also benefit to exposing more numbers of active sites. As a result, ZIF/rGO-700-AL shows higher onset potential and limiting current density than ZIF/rGO-700. ZIF/rGO-700-AL shows the same onset potential but a higher limiting current density compared with ZIF-700-AL, which proves the introduction of rGO is beneficial to the high catalytic performance. In this case, the rGO acts as a structure-directing agent to construct a continuous macroporous structure from ZIF-derived carbon nanoparticles. Additionally, the overall electrical conductivity of the catalyst would be enhanced due to the good conductive reduced graphene oxide.

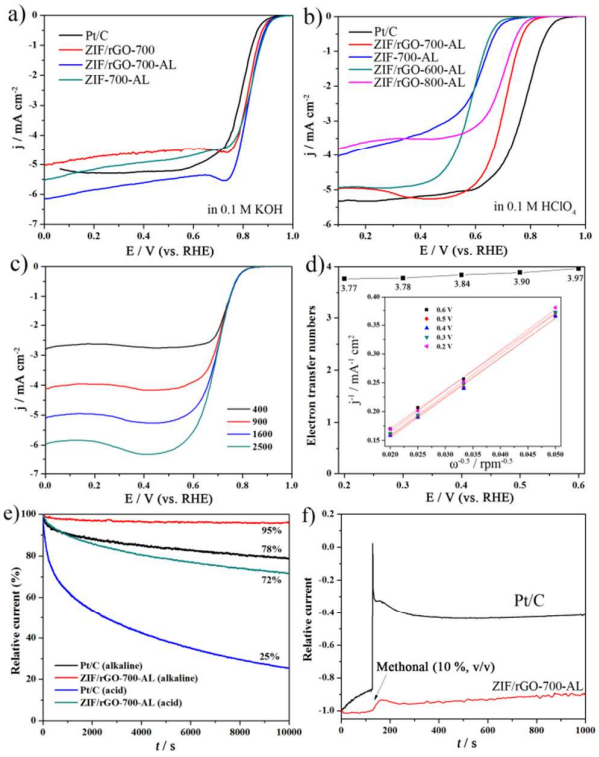

Figure 5 a) LSV curves of Pt/C, ZIF/rGO-700, ZIF/rGO-700-AL, and ZIF-700-AL at a rotation rate of 1600 rpm in O_2-saturated 0.1 M KOH solution with a scan speed of 10 mV/s. b) LSV curves of Pt/C and ZIF/rGO-700-AL at a rotation rate of 1600 rpm in O_2-saturated 0.1 M $HClO_4$ solution with a scan speed of 10 mV/s. c) LSV curves of ZIF/rGO-700-AL at various speeds in O_2-saturated 0.1 M $HClO_4$ solution. d) Electron transfer numbers of ZIF/rGO-700-AL as a functional of potentials; inset is the K-L plots at different potentials calculated from c). e) Current-time chronoamperometric response of Pt/C and ZIF/rGO-700-AL at 0.67 V in O_2-saturated 0.1 M KOH and $HClO_4$ solution. f) Chronoamperometric response of Pt/C and ZIF/rGO-700-AL at 0.67 V in O_2-saturated 0.1 M $HClO_4$ solution. The arrow indicates the introduction of 10 vol % methanol.

Generally, the ORR kinetics is more sluggish in acidic medium than alkaline medium especially for non-precious metal catalysts.[4] ZIF/rGO-700-AL was further tested as a catalyst in acidic condition (0.1 M $HClO_4$). The cathodic peaks of Pt/C and ZIF/rGO-700-AL in their CV curves are 0.80 and 0.66 V vs. RHE, respectively (Figure S3). The onset potential and limiting current density at 0.60 V of Pt/C and ZIF/rGO-700-AL from ORR curves are 0.92 V, 4.98 mA cm^{-2} and 0.83 V, 4.84 mA cm^{-2}, respectively (**Figure 5**b). ZIF/rGO-700-AL also reveals better catalytic performance than ZIF-700-AL, consistent to that in alkaline conditions. In addition, ZIF/rGO-700-AL also shows better performance than that of ZIF/GO treated with different temperatures (ZIF/rGO-600-AL and ZIF/rGO-800-AL). The overall performance of ZIF/rGO-700-AL is among the best of the contemporary Co-N_x/C ORR catalysts in both alkaline

and acidic electrolytes reported so far (Table S1). Rotation dependent limiting currents at 10 mV/s liner scan reveal that the limiting current density decreases from 5.72 to 2.84 mA cm^{-2} as the rotating speed decreases from 2500 to 400 rpm (Figure 5c). The onset potential is nearly the same. The Koutecky-Levich (K-L) plots show a good linearity and parallelism over the entire potential range (0.2 - 0.5V), indicating that their electron transfer number for ORR is similar (Figure 5d). The electron transfer numbers calculated from K-L equation are around 3.77-3.97 over the entire potential range, suggesting that the electrocatalysis exhibits a dominant four-electron oxygen reduction process.

The stability of ZIF/rGO-700-AL and commercial Pt/C was compared using chronoamperometirc measurements at 0.67 V (Figure 5e). After the reaction for 10000 s, the losses of current density are 5 % for ZIF/rGO-700-AL and 22 % for commercial Pt/C in 0.1 M KOH, which indicate a higher stability of ZIF/rGO-700-AL. When the chronoamperometirc measurements were performed in 0.1 M $HClO_4$, the current density has a much greater loss than that in alkaline solution, i.e., 28 % for ZIF/rGO-700-AL and 75 % for Pt/C. It is clear that ZIF/rGO-700-AL shows a much higher stability than Pt/C in both alkaline and acid condition. The Pt nanoparticles are susceptible to agglomeration/dissolution/Oswald ripening due to their high surface energy and weak interactions with carbon support. By contrast, the catalytically active centres (Co-N_x/C) of ZIF/rGO-700-AL modified via covalent bonding with carbon support are very stable even in acidic conditions. In the direct methanol proton exchange membrane fuel cell, the crossover of methanol from the anode to the cathode in acidic medium is quite common, and incomplete oxidation of methanol would cause the poisoning of Pt catalyst in the cathode, which inevitably reduces the reduction current. To investigate the electrocatalytic selectivity of ZIF/rGO-700-AL against the electrooxidation of methanol molecules, 10 % (v/v) of methanol was added in the 0.1 M $HClO_4$ solution saturated with O_2 during the chronoamperometirc test (Figure 5f). After adding methanol, the current density of ZIF/rGO-700-AL does not change much, except for a slight oscillation. However, the ORR current of Pt/C significantly decreases after the addition of methanol due to the methanol oxidation reaction. This result shows that ZIF/rGO-700-AL has a better methanol tolerance, and it is a promising candidate as cathode catalyst for direct methanol fuel cells.

Conclusions

In summary, we have demonstrated a graphene-directed assembly route to prepare hierarchically nanoporous Co-N_x/C materials with a macro/meso/microporous structure and high specific surface area via simple carbonization of unique ZIF nanocrystal arrays supported on GO nanosheets, followed by acid leaching to remove large Co nanoparticles. GO nanosheets are essential as a structure-directing agent for growth of ZIF nanocrystal arrays on the GO support. After carbonization, the resulting reduced graphene oxide acts as a binder to connect the ZIF-derived carbon nanoparticles into the macroporous structure formed via the shrinkage of ZIF; whereas ZIF nanocrystals are converted into meso/microporous carbon nanoparticles without any other template. The hierarchically macro/meso/microporous catalysts possess exceptional characteristics such as easily accessible active sites, highly nanoporous structure and excellent electrical conductivity; hence, they have excellent catalytic activity for ORR in both alkaline and acidic conditions. Moreover, such nanoporous Co-N_x/C catalysts exhibit superior stability and better methanol tolerance than commercial Pt/C catalysts, and therefore they are very promising in fuel cell and metal-air battery applications.

Acknowledgements

This work is supported by the Australian Research Council (Discovery Project No. DP150100765). The authors thank the staff of Monash Centre for Electron Microscopy for their technical assistance in SEM and TEM.

1 B. C. H. Steele and A. Heinzel, *Nature*, 2001, **414**, 345.
2 H. A. Gasteiger and N. M. Markovi´cacute, *Science*, 2009, 324, 48.
3 M. K. Debe, *Nature*, 2012, **486**, 43.
4 S. Gu, B. Xu, Y. Yan, *Annu. Rev. Chem. Biomol. Eng*. 2014, **5**, 429.
5 H. A. Gasteiger, S. S. Kocha, B. Sompalli and F. T. Wagner, *Appl. Catal., B*, 2005, **56,** 9.
6 V. R. Stamenkovic, B. S. Mun, M. Arenz, K. J. J. Mayrhofer, C. A. Lucas, G. Wang, P. N. Ross, N. M. Markovic, *Nat. Mater*. 2007, **6**, 241.
7 D. Wang, H. L. Xin, R. Hovden, H. Wang, Y. Yu, D. A. Muller, F. J. DiSalvo, H. D. Abruña, *Nat. Mater*. 2013, **12**, 81.
8 R. Jasinski, *Nature*, 1964, **201**, 1212.
9 M. Lefèvre, E. Proietti, F. Jaouen, J. Dodelet, *Science*, 2009, **324**, 71.
10 J. Suntivich, H. A. Gasteiger, N. Yabuuchi, H. Nakanishi, J. B. Goodenough, Y. Horn, *Nat. Chem*. 2011, **3**, 546.
11 F. Cheng, J. Shen, B. Peng, Y. Pan, Z. Tao, J. Chen, *Nat. Chem*. 2011, **3**, 79.
12 Y. Li, W. Zhou, H. Wang, L. Xie, Y. Liang, F. Wei, J. Idrobo, S. J. Pennycook, H. Dai, *Nat. Nanotechnol*. 2012, **7**, 394.
13 Q. Li, R. Cao, J. Cho, G. Wu, *Adv. Energy. Mater*. 2014, **4**, 1301415.
14 Y. Zheng, Y. Jiao, M. Jaroniec, Y. Jin, S. Z. Qiao, *Small* 2012, **8**, 3550.
15 G. Wu, P. Zelenay, *Acc. Chem. Res*. 2013, **46**, 1878.
16 S. Guo, S. Zhang, S. Sun, *Angew. Chem. Int. Ed*. 2013, **52**, 8526.
17 D. Wang, D. Su, *Energy Environ. Sci.*, 2014, **7**, 576.
18 L. Dai, L. Qu, H. Choi, J. Baek, *Chem. Rev*. 2015, 10.1021/cr5003563.
19 B. Wang, *J. Power Sources*, 2005, **152**, 1.
20 C. W. B. Bezerra, L. Zhang, K. Lee, H. Liu, A. L. B. Marques, E. P. Marques, H. Wang, J. Zhang, *Electrochimica Acta,* 2008, **53**, 4937.
21 R. L. Liu, C. von Malotki, L. Arnold, N. Koshino, H. Higashimura, M. Baumgarten and K. Müllen, *J. Am. Chem. Soc*., 2011, **133**, 10372.
22 G. Wu, K. L. More, C. M. Johnston, P. Zelenay, *Science* 2011, **332**, 443.
23 H. W. Liang, W. Wei, Z. S. Wu, X. Feng, K. Müllen, *J. Am. Chem. Soc*., 2013, **135**, 16002.

24 Z. Wu, L. Chen, J. Liu, K. Parvez, H. Liang, J. Shu, H. Sachdev, R. Graf, X. Feng, K. Müllen, *Adv. Mater*. 2014, **26**, 1450.
25 S. Li, D. Wu, H. Liang, J. Wang, X. Zhuang, Y. Mai, Y. Su, X. Feng, *ChemSusChem* 2014, **7**, 3002.
26 J. Wei, Y. Liang, X. Zhang, G. P. Simon, D. Zhao, J. Zhang, S. Jiang, H. Wang, *Nanoscale*, 2015, **7**, 6247.
27 J. Liang, R. F. Zhou, X. M. Chen, Y. H. Tang, S. Z. Qiao, *Adv. Mater*. 2014, **26**, 6074.
28 H. Liang, X. Zhuang, S. Brüller, X. Feng, K Müllen, *Nat. commun.*, 2014, **5**. 4973.
29 A. Kong, X. Zhu, Z. Han, Y. Yu, Y. Zhang, B. Dong, Y. Shan, *ACS Catal*. 2014, **4**, 1793.
30 C. Deng, H. Zhong, L. Yao, S. Liu, Z. Xu, H. Zhang, *ChemSusChem,* 2014, **7**, 3435.
31 H. Jiang, Y. Su, Y. Zhu, J. Shen, X. Yang, Q. Feng and C. Li, *J. Mater. Chem. A*, 2013, **1**, 12074.
32 S. Jiang, C. Zhu and S. Dong, *J. Mater. Chem. A*, 2013, **1**, 3593.
33 K. Niu, B. Yang, J. Cui, J. Jin, X. Fu, Q. Zhao and J. Zhang, *J. Power Sources*, 2013, **243**, 65.
34 S. Guo, W. Xia, R. Zou, L. An, D. Xia*, Energy Environ. Sci.*, 2015, **8**, 586.
35 A. Phan, C. J. Doonan, F. J. Uribe-Romo, C. B. Knobler, M. O'Keeffe, O. M. Yaghi, *Acc. Chem. Res*., 2010, **43**, 58.
36 H. L. Jiang , B. Liu , Y. Q. Lan , K. Kuratani , T. Akita , H. Shioyama ,F. Zong , Q. Xu , *J. Am. Chem. Soc.* 2011 , **133** , 11854.
37 N. L. Torad, M. Hu, Y. Kamachi, K. Takai, M. Imura, M. Naito, Y. Yamauchi, *Chem. Commun.* 2013, **49**, 2521.
38 W. Xia, A. Mahmood, R. Zou, Q. Xu, *Energy Environ. Sci*., 2015, 10.1039/C5EE00762C.
39 X. Wang, J. Zhou, H. Fu, W. Li, X. Fan, G. Xin, J. Zheng, X. Li *J. Mater. Chem. A*, 2014, **2**, 14064.
40 W. Xia, J. Zhu, W. Guo, L. An, D. Xia, R. Zou, *J. Mater. Chem. A*, 2014, **2**, 11606.
41 H. Zhong, J. Wang, Y. Zhang, W. Xu, W. Xing, D. Xu, Y. Zhang, X. Zhang, *Angew. Chem. Int. Ed*. 2014, **53,** 14235.
42 M. Jahan, Q. Bao, K. Loh, *J. Am. Chem. Soc*. 2012, **134**, 6707.
43 Y. Hou, Z. Wen, S. Cui, S. Ci, S. Mao, J. Chen, *Adv. Funct. Mater.* 2015*,* **25**, 872.
44 Y. Hou, T. Huang, Z. Wen, S. Mao, S. Cui, J. Chen, *Adv. Energy Mater*. 2014, **4**, 1400337.
45 W. Zhang, Z. Wu, H. Jiang, S. Yu, *J. Am. Chem. Soc*. 2014, **136**, 14385.
46 X. Zhou, J. Qiao, L. Yang, J. Zhang, *Adv. Energy Mater*. 2014, **4**, 1301523.
47 B. Xia, Y. Yan, X. Wang, X. Lou, *Mater. Horiz*. 2014, **1**, 379.
48 M. Liu, R. Zhang, W. Chen, *Chem. Rev.* 2014, **114**, 5117.
49 D. Geng, N. Ding, T. S. A. Hor, Z. Liu, X. Sun, Y. Zong, *J. Mater. Chem. A*, 2015, **3**, 1795.
50 W. S. Hummers Jr, R. E. Offeman, *J. Am. Chem. Soc*. 1958, **80**, 1339.

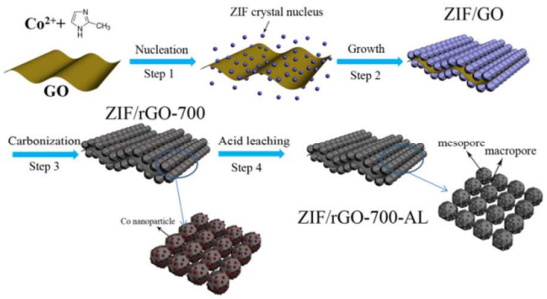

The development of non-precious metal catalysts for efficient oxygen reduction is of significance for many advanced electrochemical devices such as fuel cells and metal-air batteries. Herein, we develop a graphene-directed assembly route to synthesize hierarchically nanoporous Co-N_x/C materials with a macro/meso/microporous structure, high specific surface area (i.e. 512 m^2/g) and excellent conductivity using graphene oxide (GO) supported zeolitic imidazolate frameworks nanocrystal arrays as a catalyst precursor, followed by carbonization and acid leaching process. In this route, GO acts as a structure-directing agent to construct ZIF nanocrystal arrays supported on GO nanosheets. During the carbonization process, the resulting reduced graphene oxide functions as a binder and electrical conductor to connect individual ZIF-derived carbon nanoparticles into the macroporous structure and increase the overal conductivity. ZIF nanocrystals themselves are also converted into meso/microporous carbon nanoparticles without using any other template. The hierarchically porous Co-N_x/C materials exhibit high ORR catalytic activity, superior stability and good methanol tolerance in both alkaline and acidic conditions.